1 Response to Reviewer 1

1.1 Specific Comments

Reviewer comment: Although detailed information of the coupled radiative transfer model AccRT can be found in the literatures, I suggest to add a concise description about it in the manuscript.
Response:
The coupled radiative transfer model (AccuRT) was described twice, on line 76∼84 and 156∼179 (including Table 2), which summarizes the two in-text references, Stamnes et al., 2011 and 2018. However, because the material is split across two sections that span three complete pages, we may have missed communicating the concept clearly. Sections 1 and 2 have been reorganized in the revised version.

Reviewer comment: The method of how to construct the synthetic dataset (SD) with the coupled RTM is not clear. The detailed information about the inherit optical properties (IOPs) listed in Table 2 are needed, such as the data ranges, probability distribution, and constraints.
Response:
Physical parameters of ice, melt water on ice, and ocean water, physical parameters of snow cover, geometries, and atmospheric characteristics has been included in the revised version. As a reference, this section is included at the close of this response for your review (Tables 2∼5)) prior to our submission of the revised version.

Reviewer comment: The framework of the RTM/MLANN is not clear. I suggest to add a flowchart for it.
Response:
We are grateful for the suggestion. A flowchart has been included (Fig. 1) in the revised version.

Reviewer comment: In the manuscript, the MLANN method to used estimate the sea ice albedo. What are the performances of training, validating, and predicting accuracies of this artificial neural network model?
Response:
We have included the following statistics to the revised version of this paper: the RMSEs in training, out-of-sample validation and validation with ACLOUD data are: 0.006, 0.063, 0.099, respectively.

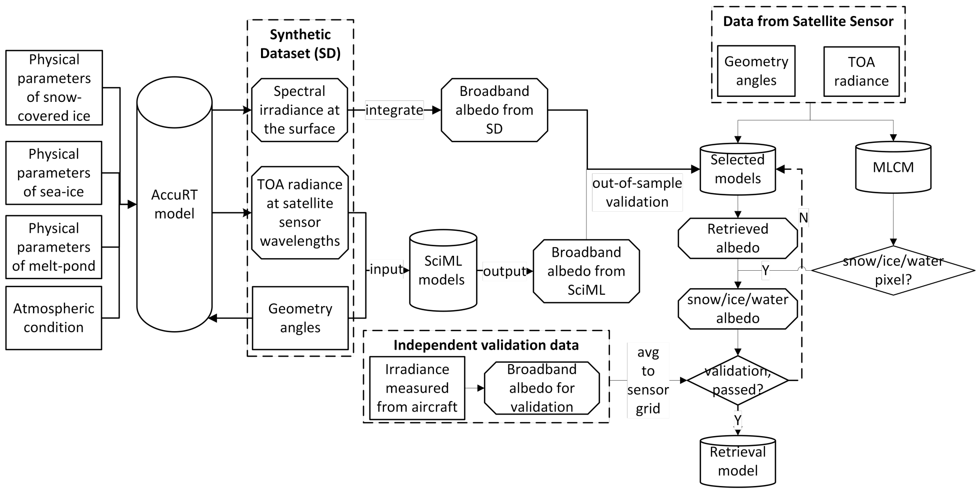

Figure 1: Flowchart of the proposed RTM/SciML framework for albedo retrieval.

Reviewer comment: The authors declared that the sensor-agnostic albedo retrieval method has the ability to apply to any optical sensor, however few explanations about this are shown in the manuscript. I suggest the authors to further explain the major theories of this method. In fact, other methods such as the MPD and direct-estimation algorithm, can also be adopted to other sensors easily. Please add a discussion about it.

Response:

The missing piece we did not include in the submitted version is how we determined the 'appropriate' channels from any optical sensor. Apart from the coupled RTM model that calculates the synthetic dataset, we use a technique to ensure that the radiance we use in practice (input from satellite channels) is consistent with that in our training data, allowing our machine learning models to be directly applied to satellite data.

The following contents have been added to the revised paper.

With our knowledge of radiative transfer theory and the differences in the radiative properties of the constituents in the coupled atmosphere-surface system, we first chose the input channels based on the following criteria:

- Avoid wavelengths with significant absorption by water vapor and/or other atmospheric constituents.

- Avoid sensor channels that have been found to be saturated in previous sensitivity investigations.

- Select wavelengths that, based on their albedo spectra, can best identify snow cover, bare ice, open water, and melt-pond surface.

With the assistance of the auto-associative neural network (AANN) technique, channels with a significant reconstruction error are deemed unsuitable for use as input to the retrieval model. More specifically, an AANN is trained using the synthetic data generated by radiative transfer model (RTM), which takes as input the three sun-satellite geometry angles as well as all radiance data that meets the aforementioned requirements and outputs all radiances. The trained AANN is believed to have picked up on the patterns in the RTM-generated dataset. Following that, the AANN is fed the same input features derived from the satellite sensor. We calculate the absolute percentage error of the reconstruction output and prune channels with an error greater than 5%.

This method is intended to avoid 'covariate shift' — a phrase used in machine learning to refer to the difference between independent variables in training and real-world data. Covariate shift is due to either (a) the saturation of certain satellite channels, which results in a much narrower dynamic range of radiance data from the satellite sensor (real world) than that calculated using RTM (training data), or (b) the response function and wide wavelength range results in a non-negligible difference between the radiance derived from the central wavelength and that obtained from the sensor. It has been demonstrated that the AANN technique is effective in detecting mismatches between data acquired for the retrieval task and data utilized for training. A recent paper[1] discusses how the AANN approach was used to identify optimal channels for retrieving ocean color products using a variety of sensors.

Similar approaches have been used to identify acceptable channels for albedo retrieval. Table 1 lists the MODIS channels that were utilized to retrieve albedo, as well as the GCOM-C/SGLI channels that were evaluated and eventually employed [2].

[1] *Fan, Yongzhen, et al. "OC-SMART: A machine learning based data analysis platform for satellite ocean color sensors." Remote Sensing of Environment 253 (2021): 112236.*

[2] Our team initially discovered the saturation issue in the 673.5 nm channel using AANN, submitted it to the GCOM-C/SGLI team, and obtained confirmation of the issue.

λ of MODIS	λ of SGLI
469	443
555	530
645	673.5*
858.5	868.5
1240	1050
1640	1630
2130	2210

Table 1: A comparison of the centre wavelengths of the channels explored and tested for the purpose of retrieving the broadband albedo at the cryosphere surface using MODIS and SGLI sensors. The 673.5 nm wavelength channel from SGLI (shown by an asterisk in the table) was proven to be saturated and hence was not used to derive albedo. Details can be found in the revised version.

Reviewer comment: The comparisons with MCD43D, MERIS, and OLCI datasets were not easily for reader to interpret. I suggested to add scatter plots to compare the differences of these datasets.

Response:

We appreciate your suggestion. Scatter plots were omitted due to the fact that the retrievals did not cover equivalent areas. For example, our cloud classification mask is stricter than those employed by OLCI and MERIS. The melt-pond detection approach does not provide values for open-water areas. Similarly, the MCD43 product returns values just along the coast. As a result, we anticipated scatter plots would be less useful than albedo maps. However, as you noted, quantitative depiction is helpful. We will explore re-griding the data and providing statistics at the geological areas specified in the revised version.

Reviewer comment: Figure 13, the authors declared that the MERIS albedo product are higher than the albedo estimated by the MLANN method in the areas with large melt pond fraction (greater than 50%). However, this difference is not obvious, and the major differences appeared in the upper right corner. Please provide an explanation for it.

Response:

Other than the wavelength difference (MERIS sensor does not have short-wave near-infrared channels), we believe the discrepancy in the area covered

by snow is due to algorithmic difference.
In our training data (the synthetic dataset created by the radiative transfer model), we explore the situation of snow-covered sea ice with snow depths ranging from 0.01∼0.2 m to 50∼150 μm (Table 4). Notably, 0.2 meter is the optically thick snow threshold. We found that the trained models use different channels and relations to retrieve the albedo of snow and ice surface. This topic is discussed in a separate paper that will be submitted shortly, in which we used the Shapley Value to deduce how these models compute albedo based on input channels and geometry angles.
The MPD-based algorithm does not discriminate between snow-covered sea ice and bare ice when retrieving albedo; both scenarios are classified as 'ice', and for both snow and ice surface, the same iterative method and the same channels were used to calculate spectral albedo. The spectral albedo is subsequently integrated to obtain broadband albedo.
In the revised version, details of how the three approaches (SciML/RTM, direct-estimation and MPD) differ in the treatment of snow-covered ice, melt-pond and bare-ice will be discussed in more detail.

Reviewer comment: Figure 13, the measurements of campaigns were not shown in this figure. Why? Please add the validation data for comparison.
Response:
The reason is that there are no campaign-measured data available to validate these results. The two locations (top and bottom) and time period (averaged between DOY 166 and DOY 170 in 2007) selected to compare the results from our algorithm and those from MERIS are the same as those used in the subsequent article:
Qu Y, Liang S, Liu Q, et al. Estimating Arctic sea-ice shortwave albedo from MODIS data[J]. Remote Sensing of Environment, 2016, 186: 32-46.
As noted in line 36∼41, Qu and Peng retrieved sea-ice albedo using the direct estimation method. Initially, we intended to utilize Qu's results as a benchmark for comparing the three algorithms. However, because we were unable to obtain the authors' original retrieval data in order to include it in the subplot, we could only show three columns in Figure 13. For your reference, Fig. 2 below shows the comparison of the three products, and the first column are screenshots of the results of Qu's algorithm, taken directly from their paper. For the second and third column, we used the same color-bar to plot the results and manually boxed the same area, but due to difference in printing and in coordinates, the colors/regions don't exactly match with

panels (a) and (b).

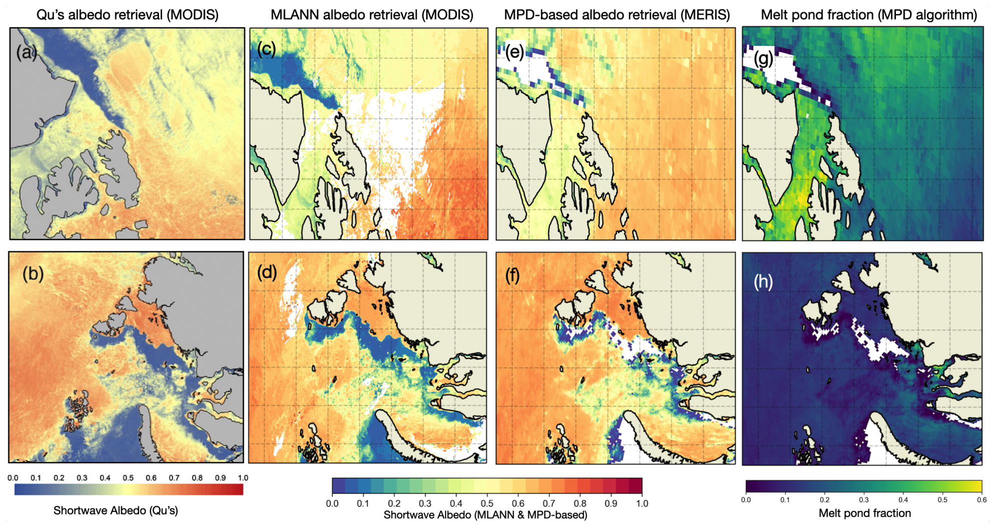

Figure 2: Maps of albedo and melt pond fraction averaged during a 5-day period in 2007 between DOY 166 and 170. From left to right: Qu's albedo retrievals, MLANN-based and MPD-based albedo retrievals, as well as the MPD-derived melt pond fraction, respectively (Qu2015Mapping, this study, and Istomina2015Melt). The upper panels depict the Banks, Prince Patrick, and Melville Islands, while the lower panels depict the Kara Sea. At the bottom, colorbars representing the corresponding values are displayed. Note that the images of Qu's retrieval results (along with the colorbar) are taken directly from Fig.10 in Qu2015Mapping, as no other data was obtainable. In panels (c) and (d), empty regions represent cloud pixels that were detected by the MLCM model (and hence removed), whereas empty regions in panels (e) through (h) represent either cloud pixels or open-water areas that were not processed by the MPD algorithm.

Reviewer comment: In the abstract, the mean absolute error (MAE) of 0.047 was used for indicating the accuracy of this method. I suggest to use root mean standard error (RMSE) to represent the estimation accuracies for the visible, near infrared, and shortwave albedo.

Response:

The text will be modified as follow to include the statistics shown in Table A2 in abstract.

In comparison to the ACLOUD campaign's albedometer measurements, the 3936 pixels of albedo retrieved under clear skies have RMSE values of 0.076, 0.137, and 0.087 in the visible, near-infrared, and short-wave bands, respectively. The RMSE is 0.099 when 7964 clear-sky pixels are compared to pyranometer observations from two aircraft during the ACLOUD campaign. The best agreement was reached on June 25th, 2017, when the campaign region experienced the least cloud cover.

1.2 Technical Corrections

Reviewer comment: Figure 7. The color ramp of this figure is not easily to interpret. Please change it.
Response:
A figure with more distinguishable colors will be presented in the next version.

Reviewer comment: Line 493, the sentences of "Istomina et al. (2015); Istomina (2020)" can be rewritten as "Istomina et al. (2015; 2020)".
Response: Revised.

Reviewer comment: Caption of Figure 13. "(Qu et al. (2015), this study, and Istomina et al. (2015))". The reference Qu et al. 2015 is not related with this figure.
Response:
Revised.

Appendix

Parameter	Sym.	Unit	Value
Sea-ice thickness	h	m	$0 \sim 3$
Brine pocket volume fraction	V_{br}	$-$	$(-0.067 \cdot \log(h) + 0.1147) \cdot (1 + 0.2 \cdot r_{\mathrm{bu}})$
Brine pocket radius	r_{br}	μm	$300 \sim 700$
Air bubble volume fraction	V_{bu}	$-$	$0.0214 \cdot h + 0.0068$
Air bubble radius	r_{bu}	μm	$-18.3 \cdot h^2 + 222.7 \cdot h + 96.5$

Table 2: Physical parameters of ice. In generating the sea-ice thickness, a truncated-normal distribution with $\mu = 0.03$, $\sigma = 1.5$ was used to ensure an adequate amount of thin ice in the SD. The brine pocket radius conforms to a Tukey-Lamdba distribution with λ=0.5.

Parameter	Units	Value
Melt water thickness	m	$0 \sim 1.5$
Chlorophyll concentrations	mg/m^3	$0.5 \sim 10$
CDOM at 443 nm	/m	$0.01 \sim 0.1$

Table 3: Physical parameters of melt water on ice and ocean water. Melt water thickness and CDOM values follow randomly-distributed uniform distributions in the specified ranges. For the chl-a concentration, a reciprocal continuous distribution (long tail extending to high values) was used.

Parameter	Symbol	Units	Value
Snow grain size	r_{e}	μm	$50 \sim 150$
Snow density	ρ_s	kg/m^3	200
Impurity fractions	$\mathrm{f}_{\mathrm{imp}}$	-	$10^{-7} \sim 10^{-6}$
Snow thickness	h_{snow}	m	$0.01 \sim 0.2$

Table 4: Physical parameters of snow cover. The snow grain size and snow thickness were generated with a randomly uniform distribution in the specified ranges.

Parameters	Value
Solar zenith angle	20$\sim$80 degrees
Sensor angle	0.01$\sim$50 degrees
Azimuth angle	0.01$\sim$180 degrees
AOD at 500 nm	$0.01 \sim 0.3$
Relative humidity	0.5
Fine mode fraction	0.9

Table 5: Geometries and atmospheric parameters. All parameters conform to random-uniform distributions in the specified ranges.